

Remote entanglement stabilization for modular quantum computing

Nicolas Didier,^{1,*} S. Shankar,² and Mazyar Mirrahimi^{1,3}

¹*QUANTIC team, Inria Paris, 2 rue Simone Iff, 75012 Paris, France*

²*Departments of Applied Physics, Yale University, New Haven, Connecticut 06520, USA*

³*Yale Quantum Institute, Yale University, New Haven, Connecticut 06520, USA*

Quantum information processing in a modular architecture requires to distribute and stabilize entanglement in a qubit network. We present autonomous entanglement stabilization protocols between two qubits that are coupled to distant cavities. The cavities coupling is mediated and controlled via a three-wave mixing device that generates either a delocalized mode or a two-mode squeezed state between the remote cavities depending on the pump frequency. Local drives on the qubits and the cavities steer and maintain the system to the desired qubit Bell state. Most spectacularly, even a weakly-squeezed state can stabilize a maximally entangled Bell state of two distant qubits through entanglement accumulation. We show that reservoir-engineering based protocols can stabilize entanglement in presence of qubit-cavity asymmetries and losses.

PACS numbers: 03.67.Pp, 03.65.Yz, 42.50.Dv, 85.25.-j, 03.65.Ud, 03.67.Bg

Introduction – Scaling up quantum machines without losing their quantumness is a challenging step toward building a quantum computer. A promising architecture is modular quantum computing, the idea is to connect long-lived small quantum units, the modules, on-demand via a quantum router [1, 2]. Modular quantum computing has a number of appealing features, among them hierarchical complexity, reconfigurability, ability to avoid cross-talks and testability [3]. Such an architecture can furthermore use quantum repeaters within the router to extend the network to a quantum internet [4].

The elementary task for modular quantum information processing is to entangle modules [5–7], more precisely to prepare and stabilize a Bell state between two distant qubits of the network. Entanglement stabilization has recently been realized experimentally for two superconducting qubits in the same cavity using bath engineering [8] and measurement-based methods [9]. The general mechanism makes use of an excited state of the cavity that decays to the qubit Bell state of interest, as depicted in Fig. 1. The cycle in Hilbert space is activated with qubit and cavity drives to prepare and stabilize the Bell state. A crucial ingredient is the symmetry of the qubit-cavity coupling required to render indistinguishable the two qubit states that superpose in the Bell state. Extending the scheme from local to distant modules requires to generate nonlocal correlations between the cavities through the router.

In this paper we propose protocols for remote entanglement stabilization that use a three-wave mixer (TWM) to couple the distant cavities containing the qubits and run the mechanisms of Fig. 1. In superconducting circuits, three-wave mixing is realized with a Josephson parametric converter [10–12], a device routinely used experimentally. It is possible to control the interaction between a pair of ports by pumping the third one; the nature and strength of the coupling is set by the pump frequency and amplitude, respectively. The TWM is a very versa-

tile device, that acts in particular as a switch with an on/off ratio in excess of 10^4 . It can be used in two modes of operation — an amplification mode with a two-mode squeezing interaction [13, 14] or a conversion mode with a beam-splitter, or tunnel, coupling [15, 16]. There are furthermore two modes of connection to the TWM, unidirectional coupling via circulators or bidirectional coupling via long resonators [17], as depicted in Fig. 1. The two remote entanglement stabilization schemes we describe in this paper correspond to two different combinations of operation and connection modes.

Amplification is obtained with a two-mode squeezing interaction, generated by the TWM for a pump frequency tuned at the frequency sum of the two other TWM modes. When the distant qubit-cavities are illuminated by this entangled light, as in Fig. 1 (a), we show that the nonlocal qubit Bell state can be stabilized with 100 % fidelity even with weak squeezing. This entanglement accumulation phenomenon is achieved when the injected two-mode squeezed state is in resonance with the cavities. Our protocol is fundamentally different from [18], that requires squeezing in resonance with the qubit frequencies and reaches high fidelities only with strong squeezing. It is moreover an entanglement *stabilization* protocol, unlike previous measurement-based remote entanglement protocols that only *prepare* entanglement without stabilizing it against decoherence [19, 20].

A beam-splitter interaction with frequency conversion is obtained when the TWM pump frequency is tuned at the frequency difference of the two other TWM modes. When the distant qubit-cavities are coupled to the TWM through long resonators, as in Fig. 1 (b), we show that the physics becomes effectively single mode. The stabilization protocol of [8] can then be applied to this delocalized mode to stabilize a nonlocal qubit Bell state. Interestingly, the crucial dispersive shift symmetry of the two qubits required in the local protocol [8] is lifted by tuning the TWM detuning. This feature distinguishes our

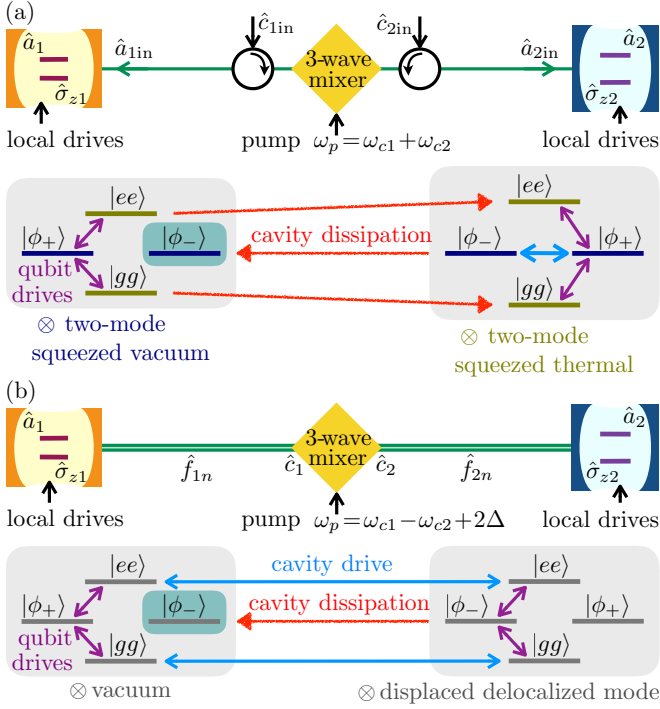


FIG. 1. Autonomous remote entanglement stabilization protocols with three-wave mixers. (a) For a directional coupling in the amplification mode, the TWM is a source of two-mode squeezed light that steers the cavities to two-mode squeezed vacuum for the even qubit subspace and to a two-mode squeezed thermal state for the odd qubit subspace. Qubit drives couple the two subspaces. A coupling between the Bell state $|\phi_{+}\rangle$ and $|\phi_{-}\rangle$ is activated by the fluctuations of the photon number imbalance present in the two-mode squeezed thermal state. Entanglement accumulation leads to the stabilization of the Bell state $|\phi_{-}\rangle$ in two-mode squeezed vacuum with 100 % fidelity. (b) For a bidirectional coupling in the conversion mode, the TWM generates delocalized modes between the two distant cavities. For large enough coupling the physics becomes effectively single mode and the protocol of Ref. 8 can be applied to a delocalized mode that is weakly sensitive to photon loss in the transmission line. The pump detuning can correct dispersive shift asymmetry.

protocol from [21, 22] that requires a symmetry on the qubits and the cavities combined with close enough cavities to get a strong tunnel coupling. Our remote entanglement protocol is furthermore robust against transmission losses, akin to population transfer in optomechanics using dark modes [23]. The better protection against transmission losses of bidirectional over directional coupling has been pointed out in [24, 25]. We describe the protocols in more details in the following and discuss their robustness against imperfections.

Two-mode squeezed states – The TWM couples the three modes \hat{c}_1 , \hat{c}_2 and \hat{c}_3 according to the Hamiltonian $\hat{H}_{\text{TWM}} = \hbar g_3(\hat{c}_1^{\dagger} + \hat{c}_1)(\hat{c}_2^{\dagger} + \hat{c}_2)(\hat{c}_3^{\dagger} + \hat{c}_3)$, where the third mode is strongly driven, it plays the role of the pump and is treated classically. Amplification is obtained for a

pump frequency ω_p set to the sum $\omega_{c1} + \omega_{c2}$ and the TWM becomes a two-mode squeezer. For directional coupling, obtained with circulators as sketched in Fig. 1 (a), the TWM acts as a correlated bath for the distant cavities. Their dissipative dynamics is governed by the Lindbladian

$$\hat{L}_S = \kappa(D[\hat{a}_1 \cosh r + \hat{a}_2^{\dagger} \sinh r] + D[\hat{a}_2 \cosh r + \hat{a}_1^{\dagger} \sinh r]), \quad (1)$$

with the dissipation superoperator $D[\hat{a}] \cdot = \hat{a} \cdot \hat{a}^{\dagger} - \frac{1}{2}\{\hat{a}^{\dagger} \hat{a}, \cdot\}$ and where we suppose the same coupling for both cavities for convenience. For empty cavities, this Lindbladian steer the cavity state to the two-mode squeezed vacuum state $\hat{\rho}_{\text{SV}} = \hat{S}_r|0,0\rangle\langle 0,0|\hat{S}_r^{\dagger}$, with the two-mode squeezing operator $\hat{S}_r = e^{r(\hat{a}_1 \hat{a}_2 - \hat{a}_1^{\dagger} \hat{a}_2^{\dagger})}$. The squeezing parameter r is set by the pump amplitude, it will be expressed in decibel in the following: $r_{\text{dB}} = (20/\log 10)r$ such that the ratio of standard deviations between the anti-squeezed and squeezed quadratures is $e^{2r} = 10^{r_{\text{dB}}/10}$.

The qubits to be stabilized are dispersively coupled to their own cavity, with the coupling Hamiltonian, $\hat{H}_{\text{dispersive},j=1,2} = -\frac{1}{2}\hbar\chi_j\hat{a}_j^{\dagger}\hat{a}_j\hat{\sigma}_{zj}$. Considering equal dispersive shifts, the qubit-cavity Hamiltonian reads

$$\hat{H}_{\text{dispersive}} = \frac{\hbar\chi}{2}\hat{N}(\hat{\sigma}_{\text{gg}} - \hat{\sigma}_{\text{ee}}) + \frac{\hbar\chi}{2}\hat{M}(\hat{\sigma}_{-+} + \hat{\sigma}_{+-}), \quad (2)$$

with $\hat{\sigma}_{kl} = |k\rangle\langle l|$, $|g\rangle = |gg\rangle$, $|e\rangle = |ee\rangle$ and $\hat{\sigma}_{-+}$, $\hat{\sigma}_{+-}$ couple the odd parity Bell states $|\phi_{\mp}\rangle = \frac{1}{\sqrt{2}}(|ge\rangle \mp |eg\rangle)$. The even and odd qubit subspaces are coupled to the photon number sum and difference, respectively,

$$\hat{N} = \hat{a}_1^{\dagger}\hat{a}_1 + \hat{a}_2^{\dagger}\hat{a}_2, \quad \hat{M} = \hat{a}_1^{\dagger}\hat{a}_1 - \hat{a}_2^{\dagger}\hat{a}_2. \quad (3)$$

Similarly to [8], the qubits are driven at resonance with the same Rabi amplitudes Ω , leading to a Hamiltonian of the form $\hat{H}_{\text{drive}} = \sqrt{2}\hbar\Omega(\hat{\sigma}_{+g} + \hat{\sigma}_{+e}) + \text{h.c.}$, coupling the even qubit subspace to $|\phi_{+}\rangle$.

To highlight the stabilization mechanism of $|\phi_{-}\rangle$ by entanglement accumulation, let us have a look at the quantum dynamics generated by the dispersive interaction Eq. (2), the qubit driving \hat{H}_{drive} , the dissipator Eq. (1) and sketched in Fig. 1 (a). Starting from the ground state of the qubits $|gg\rangle$ and the vacuum state of the cavities $|00\rangle$, the correlated dissipation combined with the dispersive coupling generate a two-mode squeezed thermal state $\hat{\rho}_{\text{ST}}$, the thermal aspect comes from the detuning of the cavities by $\chi/2$. More precisely, $\hat{\rho}_{\text{ST}} = \hat{S}_{r'}\hat{\rho}_{\text{th}}\hat{S}_{r'}^{\dagger}$, with the squeezing parameter r' defined by $\tanh 2r' = \cos\theta \tanh 2r$ and $\tan\theta = \kappa/(\chi \cosh 2r)$; The thermal population is $\bar{n}_{\text{th}} = \sinh^2 r'$ for each cavity. Qubit driving then induces oscillations between $|gg\rangle$ and $|\phi_{+}\rangle$ and the Bell state $|\phi_{-}\rangle$ is populated from $|\phi_{+}\rangle$ via the dispersive interaction. It is essential here to notice that the coupling is mediated by the photon number

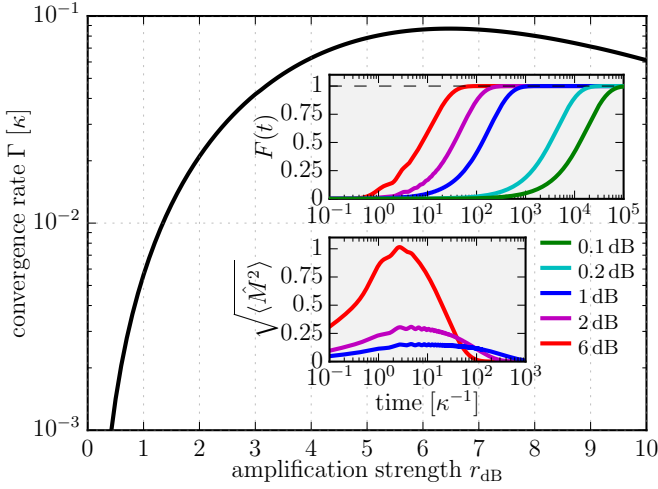


FIG. 2. Remote entanglement stabilization in the amplification mode and with the directional connection. The convergence rate is plotted versus amplification strength in dB. The optimal squeezing strength is found around 6.5 dB. Parameters are $\chi_1/2\pi = \chi_2/2\pi = 5$ MHz, $\Omega/2\pi = 0.8\kappa$, $\kappa/2\pi = 1$ MHz. Insets: Temporal dynamics of the fidelity F (top) and the fluctuations of the photon number imbalance $\sqrt{\langle \hat{M}^2 \rangle}$ (bottom) for different values of the squeezing strength.

imbalance \hat{M} , the thermal character of $\hat{\rho}_{\text{ST}}$ is thus crucial to activate this tunneling process. Indeed, the photon number imbalance is invariant under the two-mode squeezing transformation, $\hat{S}_r \hat{M} \hat{S}_r^\dagger = \hat{M}$, and hence vanishes for two-mode squeezed vacuum states. Once in the odd qubit subspace, the Lindbladian steers the cavities to the two-mode squeezed vacuum state $\hat{\rho}_{\text{SV}}$. At each round, entanglement is accumulated and the cycle in the Hilbert space stops when in $|\phi_-\rangle\langle\phi_-|\hat{\rho}_{\text{SV}}$.

The convergence rate Γ to the Bell state $|\phi_-\rangle$ is plotted in Fig. 2 versus squeezing strength. The highest rate turns out to take place at a modest squeezing strength, below 7 dB. This behavior can be explained by two competing phenomena. First, the stabilization process is activated by the fluctuations of the population imbalance \hat{M} by the two-mode squeezed thermal state; We get $\sqrt{\langle \hat{M}^2 \rangle} = \frac{1}{\sqrt{2}} \sinh 2r$ that increases with amplification strength, as shown in the inset of Fig. 2. Second, the pointer state of the cavities is a two-mode squeezed vacuum state in the odd qubit subspace and a two-mode squeezed thermal state in the even qubit subspace. The coupling between the two subspaces is performed by the qubit drive and for small drive strength, $\Omega \ll \kappa, \chi$, the oscillation rate is given by $\Omega \text{tr}\{\hat{\rho}_{\text{SV}}\hat{\rho}_{\text{ST}}\} = \Omega \langle 0,0|\hat{\rho}_{\text{th}}|0,0\rangle = \Omega [\cosh^6 r - \sinh^6 r]^{-1}$ that decreases with amplification strength. As a consequence, the stabilization rate is limited by the quantum fluctuations of \hat{M} at weak squeezing and by the distance between the cavity pointer states at large squeezing, giving rise to a

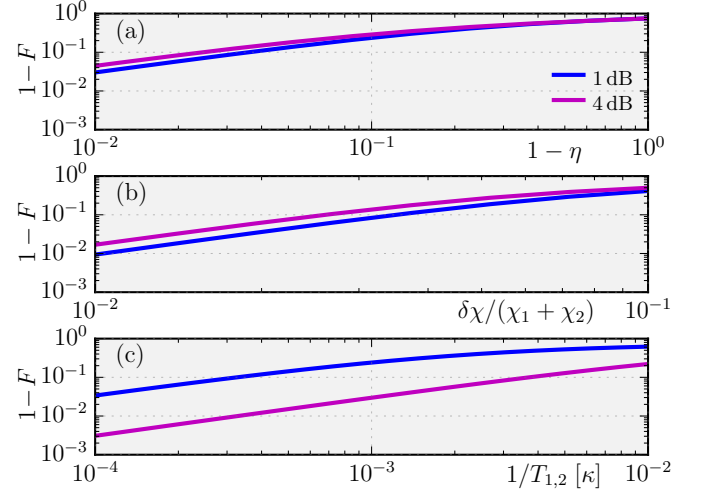


FIG. 3. Effect of imperfections on remote entanglement stabilization in the amplification mode and directional connection. Steady-state infidelity is plotted against photon losses (a), dispersive coupling asymmetry (b) and qubit dissipation $T_1 = T_2$ (c). Same parameters as in Fig. 2.

finite optimal squeezing parameter.

The effect of photon losses in the transmission lines is to heat the two-mode squeezed state for the odd qubit subspace. As a result, the two-mode squeezed vacuum state is not the steady-state and cannot stabilize the Bell state with 100% fidelity anymore. The infidelity grows linearly with the losses, as can be seen in Fig. 3 (a) (here, η represents the transmission efficiency between the TWM and each of the cavities). This situation is similar to [18] but with the crucial difference that with no loss our protocol gives a fidelity of 100%. The dispersive shift asymmetry $\delta\chi = (\chi_1 - \chi_2)$ also reduces the steady-state fidelity, but a fidelity of $F = 99\%$ is obtained for an asymmetry $\delta\chi = (\chi_1 + \chi_2)/100$, see Fig. 3 (b). The results obtained so far did not take into account the effect of qubit relaxation (rate $1/T_1$) and dephasing (rate $1/T_2$). The steady-state fidelity vanishes for dephasing rates larger than the convergence rate Γ , as plotted in Fig. 3 (c). Asymmetry in the damping rates does not significantly change the fidelity.

Delocalized mode – In the conversion mode, the pump tone frequency ω_p is set close to the difference $\omega_{c1} - \omega_{c2}$ between the frequency of the modes \hat{c}_1 and \hat{c}_2 . The TWM then generates a beam-splitter interaction,

$$\hat{H}_{\text{convert}} = \hbar\Delta(-\hat{c}_1^\dagger\hat{c}_1 + \hat{c}_2^\dagger\hat{c}_2) + \hbar g(\hat{c}_1^\dagger\hat{c}_2 + \hat{c}_2^\dagger\hat{c}_1), \quad (4)$$

in the appropriate rotating frame and after a rotating wave approximation. The detuning, $\Delta = \frac{1}{2}(\omega_p - \omega_{c1} + \omega_{c2})$, appears to be very useful to correct mismatch between the qubit-cavity couplings.

To expose the remote connection idea, as a toy model we first consider a full hybridization between the cavity mode \hat{a}_1 (\hat{a}_2) with the TWM mode \hat{c}_1 (\hat{c}_2), i.e. $\hat{c} \rightarrow \hat{a}$

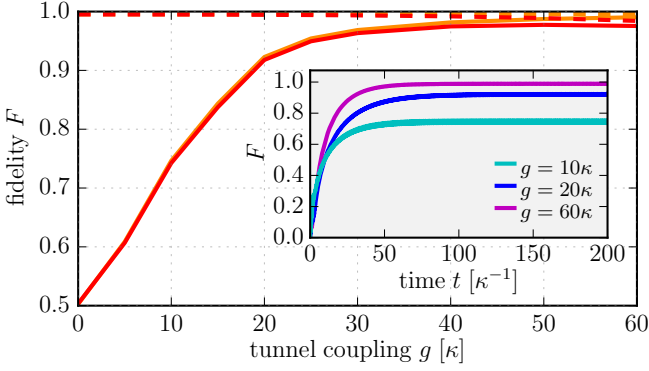


FIG. 4. Remote entanglement stabilization in the conversion mode and with the bidirectional connection. The single-cavity result (dashed line) is recovered for a sufficiently large tunnel coupling g (full line). Results are obtained for different values of the damping rate of the long resonators, $\kappa_\ell = 0$ in orange and $\kappa_\ell = 10\kappa$ in red. The damping rate of the cavities and TWM modes is $\kappa/2\pi = 1$ MHz, the effective dispersive shift is equal to $\chi_{\text{eff}} = 5\kappa$, the cavity drives are set to displace the mode \hat{d}_1 by an average of $\bar{n} = 3$ photons, the qubit drives strength is $\Omega = \kappa_{\text{eff}}/2$. For the simulations of the single-cavity case (dashed line), we vary the effective damping rate κ_{eff} similarly to the two-mode case. This explains the slight reduction of the fidelity for $\kappa_\ell = 10\kappa$ with increasing g (and therefore κ_{eff}). Inset: Temporal dynamics of fidelity establishment and stabilization for different values of the tunnel coupling and $\kappa_\ell = \kappa$.

in (4). Hamiltonian (4) is diagonalized through rotating the modes \hat{a}_j by an angle defined as $\tan 2\theta = g/\Delta$, $(\hat{d}_1 \ \hat{d}_2)^\top = R_\theta (\hat{a}_1 \ \hat{a}_2)^\top$. In order to couple the mode \hat{d}_1 to both qubits with the same dispersive shift $\chi_{\text{eff}} = \frac{\chi_1\chi_2}{\chi_1+\chi_2}$, the detuning is set to $\Delta = g \frac{\chi_1-\chi_2}{2\sqrt{\chi_1\chi_2}}$. The total Hamiltonian, (4) and (2), with the hybridized modes $\hat{d}_{1,2}$, is then given by

$$\hat{H}_{\text{toy}} = \frac{1}{2}E(\hat{d}_1^\dagger\hat{d}_1 - \hat{d}_2^\dagger\hat{d}_2) - \frac{1}{2}\hbar\chi_{\text{eff}}(\hat{\sigma}_{z1} + \hat{\sigma}_{z2})\hat{d}_1^\dagger\hat{d}_1, \quad (5)$$

with the energy separation $E = \hbar g \frac{\chi_1+\chi_2}{\sqrt{\chi_1\chi_2}}$. For a tunnel coupling g strong enough to ensure $E \gg \hbar\chi_{\text{eff}}$, the delocalized mode \hat{d}_2 is largely detuned from \hat{d}_1 . As a consequence, we have neglected the coupling between \hat{d}_1 and \hat{d}_2 through the dispersive interaction. The physics becomes effectively single mode and the protocol experimentally realized in [8] can be applied to the delocalized mode \hat{d}_1 . Manipulating mode \hat{d}_1 is straightforwardly achieved with drives on one or both cavities. The final Hamiltonian after a rotating wave approximation in the large tunnel coupling g limit in the interaction picture reads

$$\begin{aligned} \hat{H}_{\text{eff}} = & \chi_{\text{eff}}(\hat{\sigma}_{\text{gg}} - \hat{\sigma}_{\text{ee}})\hat{d}_1^\dagger\hat{d}_1 + \kappa\sqrt{\bar{n}}\cos(\chi_{\text{eff}}t)(\hat{d}_1^\dagger + \hat{d}_1) \\ & + \{\Omega(\hat{\sigma}_{+g} + \hat{\sigma}_{+e}) - \Omega e^{i\bar{n}\chi_{\text{eff}}t}(\hat{\sigma}_{-g} - \hat{\sigma}_{-e}) + \text{h.c.}\}. \end{aligned} \quad (6)$$

The first term of Hamiltonian \hat{H}_{eff} shifts the frequency of the cavities by $\pm\chi_{\text{eff}}$ if the qubits are both in ground

or excited state, but does not involve the qubit states $|ge\rangle$ and $|eg\rangle$ that contribute to the Bell state to be stabilized. This crucial property is the result of correcting the dispersive shift asymmetry with Δ . The second term displaces the cavity states to a coherent state with an average of \bar{n} photons if the qubits are in states $|gg\rangle$ or $|ee\rangle$, it corresponds to the cavity drive channel in Fig. 1 (b). The last terms drive the qubit to the Bell state $|\phi_+\rangle$ if the cavities are empty and to the Bell state $|\phi_-\rangle$ if the cavities are displaced, respectively. Both cavities are also coupled to zero-temperature environments with damping rate κ , that tends to relax the cavities to vacuum. The resulting quantum dynamics stabilizes the state $|\phi_-\rangle|00\rangle$. The fidelity F of the Bell state $|\phi_-\rangle$ is plotted in Fig. 4 versus tunnel coupling strength and compared to the result obtained for two qubits in the same cavity [8]. The remote entanglement stabilization converges to the local protocol result for $g \gtrsim 40\kappa$. In this limit, the characteristics of the stabilization process have been widely studied for a single cavity [9, 26] and can be directly used to describe the remote configuration. Temporal dynamics for the preparation and stabilization protocol are plotted in the inset of Fig. 4.

We now consider the cavities coupled to the TWM through long resonators, described by the harmonics \hat{f}_{1n} and \hat{f}_{2n} of fundamental frequency well below the cavity and TWM frequencies [17]. Among those let us select the closest harmonic to each cavity frequency, \hat{f}_1 and \hat{f}_2 , and consider for simplicity that the three modes \hat{a}_1 (\hat{a}_2), \hat{f}_1 (\hat{f}_2), \hat{c}_1 (\hat{c}_2) are in resonance. We note $\tilde{g}\sin\varphi$ the coupling between modes \hat{a}_1 (\hat{a}_2) and \hat{f}_1 (\hat{f}_2) and $\tilde{g}\cos\varphi$ the coupling between \hat{f}_1 (\hat{f}_2) and \hat{c}_1 (\hat{c}_2). Very interestingly, in the limit of large coupling to the long resonators $\tilde{g} \gg g, \Delta$, the dynamics can be restricted to the two delocalized modes \hat{d}_1, \hat{d}_2 involving the cavity and TWM modes with a vanishing contribution of the connecting modes. The modes $\hat{d}_{1,2}$ are weakly dependent on the dissipation κ_ℓ of the long resonators, they are thus delocalized dark modes with respect to the connecting resonators. The resulting effective Hamiltonian is similar to Eq. (5) with parameters $E = g \frac{\chi_1+\chi_2}{\sqrt{\chi_1\chi_2}} \sin^2\varphi$ and $\chi_{\text{eff}} = \frac{\chi_1\chi_2}{\chi_1+\chi_2} \cos^2\varphi$. For similar dispersive shifts and coupling strengths and for large enough tunnel coupling, the physics is equivalent to the single cavity realization [8] but with an effective dispersive coupling that is divided fourfold; The extension to remote cavities thus requires strong dispersive couplings, $\chi_{1,2} \sim 20\kappa$.

A more rigorous description of the whole system, involving the harmonics $\hat{f}_{1,2n}$, shows that the effective single mode description is valid for large enough tunnel coupling g and away from other resonances [27]. In Fig. 4 the parameters of the delocalized modes \hat{d}_1 and \hat{d}_2 are obtained after diagonalization of the linear system. The cavity frequencies are $\omega_{c1}/2\pi = 7$ GHz, $\omega_{c2}/2\pi = 11$ GHz, the dispersive shifts are $\chi_1/2\pi = 18.8$ MHz and

$\chi_2/2\pi = 15$ MHz, the fundamental frequency of the long resonators is $\omega_{f0} \simeq 1$ GHz, the detuning between the cavities and the TWM modes is set to ± 10 MHz, as for the detuning between the cavity mode \hat{a}_1 (\hat{a}_2) and the 7th (11th) harmonic $\hat{f}_{1,7}$ ($\hat{f}_{2,11}$), the coupling to the long resonators is $\tilde{g}/2\pi = 100$ MHz with $\varphi = 0.22\pi$. Concerning the robustness to imperfections, the pump detuning is used to correct a dispersive coupling asymmetry and an asymmetry in other parameters does not lead to qualitative changes in performances. Only a large damping rate of the connecting resonators, $\kappa_\ell = 10\kappa$, can affect the stabilized fidelity (see Fig. 4).

Conclusion – We have proposed two protocols for entanglement stabilization of two distant qubits that are connected via a router based on a three-wave mixing device. Entanglement preparation and stabilization is fully controlled by the TWM pump amplitude and frequency. The stabilization mechanisms use different non-local resources, either a two-mode squeezed state or a delocalized mode. The latter protocol is more robust against experimental imperfections such as asymmetries and losses. However with the protocol using a shared two-mode squeezed state, even modest squeezing results in significant entanglement. Our protocols are very general and can be implemented in circuit QED with current technologies. Remote entanglement stabilization based on TWMs can be used to distribute entanglement in a qubit network and is hence well suited for modular quantum computing. TWMs turn out to be advantageous devices for quantum communications and can furthermore be used together with quantum repeaters to build a quantum internet network.

Acknowledgements – We gratefully acknowledge useful discussions with Aashish Clerk, Michel Devoret and Benjamin Huard. This research was supported by the Agence Nationale de la Recherche under grant ANR-14-CE26-0018, by Inrias DPEI under the TAQUILLA associated team and by ARO under Grant No. W911NF-14-1-0011.

* Current address: Rigetti Quantum Computing, 775 Heinz Avenue, Berkeley, California 94710, USA.

- [1] C. Monroe, R. Raussendorf, A. Ruthven, K. R. Brown, P. Maunz, L.-M. Duan, and J. Kim, Phys. Rev. A **89**, 022317 (2014).
- [2] S. Debnath, N. M. Linke, C. Figgatt, K. A. Landsman, K. Wright, and C. Monroe, Nature **536**, 63 (2016).
- [3] C. R. Monroe, R. J. Schoelkopf, and M. D. Lukin, Sci. Am. **314**, 50 (2016).
- [4] H. J. Kimble, Nature **453**, 1023 (2008).
- [5] D. Gottesman and I. L. Chuang, Nature **402**, 390 (1999).
- [6] J. Eisert, K. Jacobs, P. Papadopoulos, and M. B. Plenio, Phys. Rev. A **62**, 052317 (2000).
- [7] L. Jiang, J. M. Taylor, A. S. Sørensen, and M. D. Lukin, Phys. Rev. A **76**, 062323 (2007).
- [8] S. Shankar, M. Hatridge, Z. Leghtas, K. M. Sliwa, A. Narla, U. Vool, S. M. Girvin, L. Frunzio, M. Mirrahimi, and M. H. Devoret, Nature **504**, 419 (2013).
- [9] Y. Liu, S. Shankar, N. Ofek, M. Hatridge, A. Narla, K. M. Sliwa, L. Frunzio, R. J. Schoelkopf, and M. H. Devoret, Phys. Rev. X **6**, 011022 (2016).
- [10] N. Bergeal, F. Schackert, M. Metcalfe, R. Vijay, V. E. Manucharyan, L. Frunzio, D. E. Prober, R. J. Schoelkopf, S. M. Girvin, and M. H. Devoret, Nature **465**, 64 (2010).
- [11] N. Roch, E. Flurin, F. Nguyen, P. Morfin, P. Campagne-Ibarcq, M. H. Devoret, and B. Huard, Phys. Rev. Lett. **108**, 147701 (2012).
- [12] B. Abdo, A. Kamal, and M. Devoret, Phys. Rev. B **87**, 014508 (2013).
- [13] E. Flurin, N. Roch, F. Mallet, M. H. Devoret, and B. Huard, Phys. Rev. Lett. **109**, 183901 (2012).
- [14] E. Flurin, N. Roch, J. D. Pillet, F. Mallet, and B. Huard, Phys. Rev. Lett. **114**, 090503 (2015).
- [15] B. Abdo, K. Sliwa, F. Schackert, N. Bergeal, M. Hatridge, L. Frunzio, A. D. Stone, and M. Devoret, Phys. Rev. Lett. **110**, 173902 (2013).
- [16] A. J. Sirois, M. A. Castellanos-Beltran, M. P. DeFeo, L. Ranzani, F. Lecocq, R. W. Simmonds, J. D. Teufel, and J. Aumentado, Appl. Phys. Lett. **106**, 172603 (2015).
- [17] N. M. Sundaresan, Y. Liu, D. Sadri, L. J. Szöcs, D. L. Underwood, M. Malekakhlagh, H. E. Türeci, and A. A. Houck, Phys. Rev. X **5**, 021035 (2015).
- [18] B. Kraus and J. I. Cirac, Phys. Rev. Lett. **92**, 013602 (2004).
- [19] N. Roch, M. E. Schwartz, F. Motzoi, C. Macklin, R. Vijay, A. W. Eddins, A. N. Korotkov, K. B. Whaley, M. Sarovar, and I. Siddiqi, Phys. Rev. Lett. **112**, 170501 (2014).
- [20] M. Silveri, E. Zalus-Geller, M. Hatridge, Z. Leghtas, M. H. Devoret, and S. M. Girvin, Phys. Rev. A **93**, 062310 (2016).
- [21] C. Aron, M. Kulkarni, and H. E. Türeci, Phys. Rev. A **90**, 062305 (2014).
- [22] M. E. Kimchi-Schwartz, L. Martin, E. Flurin, C. Aron, M. Kulkarni, H. E. Türeci, and I. Siddiqi, Phys. Rev. Lett. **116**, 240503 (2016).
- [23] Y.-D. Wang and A. A. Clerk, Phys. Rev. Lett. **108**, 153603 (2012).
- [24] F. Motzoi, E. Halperin, X. Wang, K. B. Whaley, and S. Schirmer, Phys. Rev. A **94**, 032313 (2016).
- [25] Z. Shi and H. I. Nurdin, Quant. Inf. Process. **14**, 337 (2015).
- [26] Z. Leghtas, U. Vool, S. Shankar, M. Hatridge, S. M. Girvin, M. H. Devoret, and M. Mirrahimi, Phys. Rev. A **88**, 023849 (2013).
- [27] See Supplemental Material.